https://doi.org/10.3311/PPee.22147

Periodica Polytechnica Electrical Engineering and Computer Science, 68(2), pp. 157–167, 2024

Adaptive Hierarchical Fractional-Order Sliding Mode Control Strategy for Multi-terminal VSC-HVDC System with Wind Farm

Dipak Ranjan Swain[1], Sunita S. Biswal[2*], Pravat K. Rout[2], Prakash K. Ray[1], Ranjan K. Jena[1]

[1] Department of Electrical Engineering, College of Engineering and Technology, Odisha University of Technology and Research (OUTR), Ghatikia, Kalinga Nagar, Bhubaneswar 751003, Odisha, India
[2] Department of Electrical and Electronics Engineering, Faculty of Engineering Technology, Siksha 'O' Anusandhan (SOA), Khandagiri, Bhubaneswar 751030, Odisha, India
* Corresponding author, e-mail: sunitabiswal@soa.ac.in

Received: 04 March 2023, Accepted: 12 January 2024, Published online: 03 April 2024

Abstract

In this paper, an adaptive hierarchical fractional-order sliding mode controller (AHFSMC) for a multi-terminal Voltage Source Converter (VSC) based High Voltage Direct Current (HVDC) Integrated with a wind farm (WF) system is designed. Multi-terminal VSC-HVDC (MtVDC) connected to wind farms has received several attentions in the power sector because of its numerous benefits. The effectiveness of MtVDC, on the other hand, is dependent on the control scheme used. To achieve this goal, a hierarchical sliding mode control method by fractional-order calculus is used. The controller parameters are adjusted according to a suitable adaptation method to enhance the proposed controller's robustness compared to the system uncertainties coefficient. An appropriate Lyapunov-based approach is used to achieve the adaptation rule. This paper discusses a scheme to design additional controllers in MtVDC systems to damp electromechanical oscillations, one of several features of HVDC presently under active study. Numerical simulations validate the proposed control strategy's feasibility and efficiency. This novel approach is employed for the upgrading of system stability with the dynamic properties of the MtVDC in a variety of operative conditions.

Keywords

voltage-source converter, high voltage direct current, hierarchical fractional sliding mode controller, wind farm

1 Introduction

The world is in transition, and energy is at the heart of it. Since 2000, India has been responsible for nearly 10% of the increase in global energy demand [1]. Therefore, currently, the country intends to significantly increase the proportion of renewable energy sources (ReS) used to provide its electricity consumption. According to studies in India, wind power is achieving popularity among other types of ReSs.

According to the MNRE, Government of India, out of 7 windy states Madhya Pradesh has a lower wind potential rate. Madhya Pradesh Power Management Company Ltd has shown consistent growth in terms of renewable capacity addition in its efforts to contribute to the achievement of national renewable targets [2]. There are many wind farms (WF) in MP among which Mamatkheda WF is an onshore wind power project with a capacity of 100.5 MW. The project consists of 67 1.5 MW WTGs which generates 180 GWh of clean electricity per year, enough to power 42.000 households [3]. The use of HVDC technology to upgrade the Mamatkheda power grid [4] will allow for an enormous perception of renewable energy without jeopardizing the power system stability. Voltage source converter-based High Voltage Direct Current (VSC-HVDC) technology are currently associated to green energy to include wide range renewable energy plants.VSC-HVDC systems allows for the system interconnectedness operating at dissimilar frequencies, and the system has no problems with angular stability. There are numerous advantages to constructing a multi-terminal VSC-HVDC (MtVDC) system rather than other transmission systems [5].

The use of MtVDC technology in India's electric power grid will allow for high integration of wind power without jeopardizing the power system and voltage stability, active and reactive power flow, and power quality. However, intrinsic nonlinearity of the MtVDC system with WF cannot be disregarded when transient disturbances occur. The operation and control of an MtVDC system remains

Cite this article as: Swain, D. R., Biswal, S. S., Rout, P. K., Ray, P. K., Ranjan, K., Jena, R. K. "Adaptive Hierarchical Fractional-Order Sliding Mode Control Strategy for Multi-terminal VSC-HVDC System with Wind Farm", Periodica Polytechnica Electrical Engineering and Computer Science, 68(2), pp. 157–167, 2024. https://doi.org/10.3311/PPee.22147

an open and challenging problem. As a result, a nonlinear, adaptive, and robust controller design is required to improve the transient stability of MtVDC.

Therefore, this study explores further its control strategy formulation. Among the various nonlinear control schemes, SMC is a sophisticated technique with elegant features such as better stability, faster response, and significant robustness [6]. This control technique is notable for its ease and high accuracy, making it appropriate for wind power generation systems. The chattering problem and high-frequency switching close to the sliding surface generated by the discontinuous control law in SMC design and parasitic dynamics interactions are the key drawbacks of SMC techniques.Based on SMC, for each state variable, hierarchical sliding mode control (HSMC) may create the first layer sliding surfaces, which are then combined to create the second layer sliding surface. In recent times, researchers have focused on using fractional calculus [7]. The usage of fractional calculus can aid in the elimination of external interference and steady-state error. Adding fractional order in hierarchical SMC results in an SMC structure with fractional-order operators improve control performance. Furthermore, Fractional Lyapunov or adaptive FHSMC (AFHSMC) results can be used to calculate the asymptotic stability of fractional-order systems and also deal with model system uncertainties and external disturbances better [8]. In this study, proposed AFHSMC has been used to control the parameters of an MtVDC links on the dynamics of the Mamatkheda system.

The remainder of the paper's presentation is structured as follows: Section 2 introduces the test system model of the proposed approach with the VSC-HVDC mathematical model. Section 3, describes the proposed control strategy's design process based on the adaptive FHSMC control concept concerning MtVDC dynamics. Simultaneously, the controller's stability is examined. Section 4 demonstrates, the controller's feasibility through the simulation results and compares it with the other approaches. Section 5 contains the conclusions.

2 Modeling of the simulated test system

An MtVDC system has four terminals; each converter station are connected via transport cables for the DC portion. A WF is linked to the collector line by a generator, and then to the MtVDC system. VSC-1 controls the amplitude and frequency of the alternating current (AC) voltage as shown in Fig. 1 VSC-3 controls a steady DC voltage.

The system parameters' values are presented in Appendix.

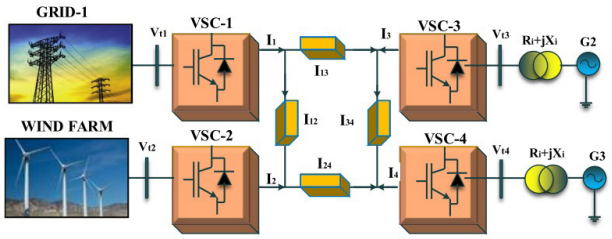

Fig. 1 The power system model under study

2.1 VSC-HVDC dynamics mathematical modelling

The mathematical representation referring to the dynamics and operation in the time domain of synchronous generators, both of the stations are given in the paper [9].

Dynamic modeling of VSC-1:

$$\begin{cases} \dfrac{dI_{rD1}}{dt} = -\dfrac{R_{r1}}{L_{r1}} I_{rD1} + wI_{rQ1} + \dfrac{(mV_{D1})}{L_{r1}} - \dfrac{V_{rD1}}{L_{r1}} \\ \dfrac{dI_{rQ1}}{dt} = -\dfrac{R_{r1}}{L_{r1}} I_{rQ1} - wI_{rD1} + \dfrac{(mV_{Q1})}{L_{r1}} - \dfrac{V_{rQ1}}{L_{r1}} \end{cases}, \tag{1}$$

Eq. (1) becomes Eq. (2) when uncertainty components are included:

$$\begin{cases} \dfrac{dI_{rD1}}{dt} = F_d\left(I_{rD1}, I_{rQ1}, V_{D1}, V_{rD1}\right) + zm_d + \sigma_d \\ \dfrac{dI_{rQ1}}{dt} = F_q\left(I_{rD1}, I_{rQ1}, V_{D1}, V_{rD1}\right) + zm_q + \sigma_q \end{cases}, \tag{2}$$

$$\frac{dV_{dc_1}}{dt} = \frac{P_{dc_1}}{C_{dc}V_{dc_1}} - V_{dc_1}\left(\frac{1}{C_{dc}R_{dc}}\right) + V_{dc_2}\left(\frac{1}{C_{dc}R_{dc}}\right). \tag{3}$$

The AC bus voltage at both of the station end in terms of d–q axis decomposition is denoted as V_{D1} and V_{Q1} respectively. The AC-DC output voltages and currents at VSC-1 in terms of d–q axis decomposition are denoted as V_{rD1}, V_{rQ1}, I_{rD1} and I_{rQ1} respectively. The equivalent resistance and inductance at VSC-1 are denoted as R_{r1} and L_{r1} respectively. The m is the modulation index and $z = (V_{dc1}/2\ L_{r1})$. The DC-link capacitance is denoted as C_{dc}. The DC transmission line resistance is denoted as R_{dc}. The σ_d and σ_q are the model uncertainties. The DC bus voltages across the DC link capacitors at both of the station regions are denoted as V_{dc1} and V_{dc2} respectively. The active and reactive power transferred at rectifier station ends of VSC-1 from the generator are denoted as P_1 and Q_1 respectively. The flow of active and reactive power from the generator to the VSC-1 of the rectifier station end can be expressed as in Eq. (4):

$$P_1 = V_1 I_{1q} \text{ and } Q_1 = V_1 I_{1d}. \tag{4}$$

The reactive and active powers can be represented for the converter station as follows:

$$P_r = V_{rD1}I_{rD1} + V_{rQ1}I_{rQ1},\ Q_r = -V_{rD1}I_{rQ1} + V_{rQ1}I_{rD1}. \quad (5)$$

In this simulation, the positive power flow direction is chosen as the direction from the wind farm towards the VSC-1 of the rectifier.

3 Design of controller

This section provides a brief description of all the controllers used in this study. By providing a comparative study of the results, the sliding mode controller (SMC), fractional SMC (FSMC), and hierarchical FSMC (HFSMC) controllers are considered to explain the efficacy of the proposed approach.

3.1 Sliding Mode Controller (SMC)

Sliding mode control is a variable structure control scheme renowned for its resistance to instabilities and parameter changes. Because power electronic converters intrinsically involve switching devices, this is a perfect solution for implementing a control that takes advantage of the power electronic converter's nonlinear nature. However, the chattering effect, which is caused by the contact of high-frequency switching and the parasitic dynamics of the system, limits its application in systems demanding high dynamic performance. Furthermore, standard SMC cannot guarantee finite-time convergence. The sliding mode asymptotic stability is ensured by the linear sliding surface in Eq. (6) with the rate of convergence based on the value of *c*. The classical linear sliding surfaces have been shown to perform poorly regarding convergence rate and settling time. The disadvantages of linear SMC were overcome through hybridization to create or by modifying the reaching law. The use of nonlinear sliding surfaces can improve the dynamic response of a closed-loop system:

$$s = cx_1 + x_2,\ c > 0. \quad (6)$$

An integrator is added to the control loop to remove the steady-state inaccuracy of sliding mode control. In the *dq* frame, the positive system sliding surfaces $s + d$ and $s + q$ are chosen according to Eq. (6):

$$s_d = k_{pd} \times e_d(t) + k_{id} \int e_d(t) \quad (7)$$

$$s_q = k_{pq} \times e_q(t) + k_{iq} \int e_q(t), \quad (8)$$

where the sliding faces' control parameters are k_{pd}, k_{id}, k_{pq}, and k_{iq}. In this study, a controller is utilized for the rectifier station i.e.VSC-1. The corresponding errors signifying the disturbance and change of system parameters are as follows:

$$\begin{cases} e_d = -I_{rD1ref} + I_{rD1} \\ e_q = -I_{rQ1ref} + I_{rQ1} \end{cases}. \quad (9)$$

Traditional sliding mode controls exhibit a high-frequency chattering problem that can be cracked by using the exponential reaching law through saturated function sat (.). The gain parameters of SMC controllers are needed to be tuned under the change in conditions and are complex. So, it is necessary to design with a balanced setup as each parameter influences the performance differently.

3.2 Fractional Sliding Mode Controller (FSMC)

The fractional-order sliding surface is one more nonlinear sliding surface strategy that employs fractional calculus in the construction of its sliding surface. Fractional-order terms are more stable because they attenuate old data while storing new data. These controllers have the potential to produce an open-loop transfer function through a fractional-order integrator, resulting in a controlled system that is resistant to changes in process gain and also have a higher degree of freedom than integral order controllers, resulting in superior dynamic performance and more robust control designs.

3.2.1 Fractional calculus prefaces

Conventional controllers created with the help of fractional order calculus result in a design that is more robust and adaptable that meets the system requirements. Fractional calculus has three common definitions among which the Riemann-Liouville (RL) type calculus definition is used in this study.

Definition-1: The fractional integral of α order of a continuous function $f(t)$ defined by Riemann–Liouville (RL) expressions is as follows:

$${}_rD^{-\alpha} f(t) = L^{\alpha}(t) = \frac{1}{\Gamma(\alpha)} \int_r^t (t-\tau)^{\alpha-1} f(\tau) d\tau,\ \alpha \in r^+, \quad (10)$$

where $L^{\alpha}(t)$ is fractional-order integral operator.

Definition-2: The fractional differential of α order of a continuous function $f(t)$ defined by Riemann–Liouville (RL) expressions is as follows:

$$\begin{aligned} {}_rD_t^{\alpha} \times f(t) &= D^n \left({}_0D_t^{\zeta} f(t) \right) \\ &= \frac{1}{\Gamma(\zeta)} \frac{d^n}{dt^n} \int_0^t (t-\tau)^{\zeta-1} f(\tau) d\tau, \end{aligned} \quad (11)$$

where ${}_rD_t^\alpha$ is fractional-order differential operator, $0 < \alpha < 1$ and $\zeta = n - \alpha$, n is the first integer that is greater than α. Γ(.) is the Euler's Gamma function:

$$\Gamma(a) = \int_0^\infty x^{\alpha-1} e^{-x} dx. \tag{12}$$

Theorem 1: The Laplace transform is a widely used tool in the analysis and design of control systems. The RL fractional calculus Laplace transform is:

$$L\left[{}_rD_t^\alpha \times f(t)\right] = s^\alpha F(s) - \sum_{i=0}^{n-1}\left[{}_rD_t^{\alpha-i-1} f(t)\right]_{t=0} s^i, \tag{13}$$

where Laplace operator is s and $n - 1 < \alpha < n$ and $n \in Z$.

Theorem 2: Consider the Prabhakar fractional integral's Laplace transform with $t_0 = 0$. Prabhakar's operator for cracking a specific particular integral equation has also been adjusted as a fractional differential integral operator, and its characteristics and utilization have been examined in research work such as [10]. The fractional integral of Prabhakar is defined as:

$$\int_a^x (x-y)^{\mu-1} E_{\eta,\mu}^\rho \left\{\nu (x-y)^\eta\right\} f(y) dy, \quad \Re e(\eta) > 0, \ \Re e(\mu) > 0, \tag{14}$$

where integration constant is a and μ, η, ν, $\rho \in C$ is the constant parameters. The Mittag-leffler function is:

$$E_{\eta,\mu}^\rho(x) = \sum_{k=0}^\infty \frac{(\rho)_k x^k}{\Gamma(\eta k + \mu) k!}. \tag{15}$$

For a full description of the Mittag-Leffler function features, generalisations, and applications the reader should see [11]. Non-linear processes have already found applications for Prabhakar operators. Prabhakar function, as well as several of its extensions, been numerically computed in the full complex plane. The Prabhakar function's Laplace transform is

$$k! \frac{s^{\eta\rho-\mu}}{\left(s^\eta - \eta\right)^{k+1}}. \tag{16}$$

3.2.2 Design of FSMC

As shown in Section 2, the MtVDC system is a composite nonlinear system whose parameters differ depending on a variety of factors. To ensure optimal performance, a robust controller is essential to cope with these ambiguities and variances. The dynamics of the sliding mode are, nevertheless, regulated by integer-order differential equations in those approaches. Integer calculus is extended to fractional calculus or Fractional based differential equations (FDEs) and is more accurate than integer-based differential equations in describing system dynamics. Motivated by this fact, the MtVDC system proposes a SMC with a sliding surface of fractional integer order (PI^α). In theory, when compared to sliding surfaces that decay exponentially towards zero, fractional-order sliding surfaces have steady energy transfer during switching, resulting in less chattering. Fig. 2 depicts the FSMC principle model.

The fractional PI sliding surface is given in Eq. (17), where ${}_0D_t^{-\alpha}(.)$ is a fractional integration of order α. A classical integer-order PI sliding surface for VSC-1 in d and q control is obtained by setting α:

$$\begin{cases} s_d(t) = k_{pd} \times e_d(t) + k_{id} \times {}_0D_t^{\alpha-1} e_d(t), \\ k_{pd}, k_{id} > 0 \quad 0 < \alpha < 1 \\ s_q(t) = k_{pq} \times e_q(t) + k_{iq} \times {}_0D_t^{\alpha-1} e_q(t), \\ k_{pq}, k_{iq} > 0 \quad 0 < \alpha < 1 \end{cases} \tag{17}$$

where the sliding faces' gain parameters are k_{pd}, k_{id}, k_{pq}, and k_{iq}. Equations (7) and (8) can be rewritten as:

$$\begin{cases} s_d = k_{pd} \times e_d + k_{id} \times {}_0D_t^{\alpha-1}\left(\text{sign}\left(e_d\right)^\gamma\right), \quad \gamma < 1 \\ s_q = k_{pq} \times e_q + k_{iq} \times {}_0D_t^{\alpha-1}\left(\text{sign}\left(e_q\right)^\gamma\right), \end{cases}. \tag{18}$$

By taking the derivative of Eq. (18) and substituting the e_d and e_q from Eq. (9) into Eq. (18), the equations of the sliding of the surface can be written as:

$$\begin{cases} \dot{s}_d = k_{pd}\left(\dot{I}_{rD1} - \dot{I}_{rD1ref}\right) + k_{id}\, {}_0D_t^\alpha \text{sign}\left(e_d\right)^\gamma \\ \dot{s}_q = k_{pq}\left(\dot{I}_{rQ1} - \dot{I}_{rQ1ref}\right) + k_{iq}\, {}_0D_t^\alpha \text{sign}\left(e_q\right)^\gamma \end{cases}. \tag{19}$$

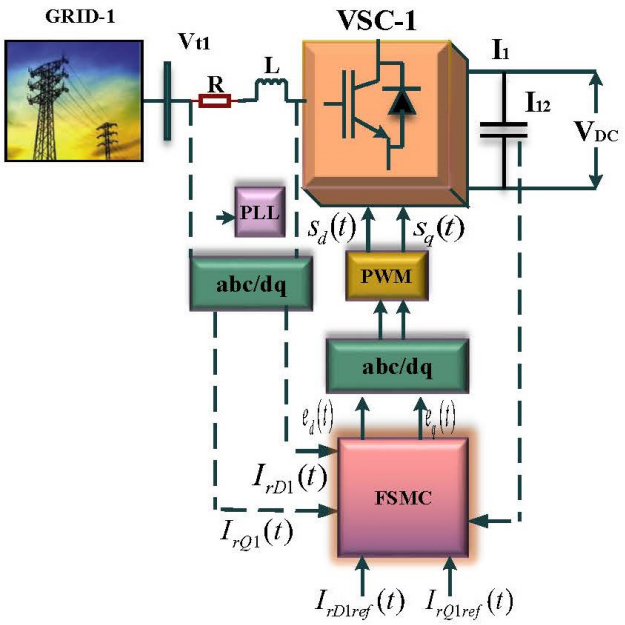

Fig. 2 The principle model of FSMC

Here $\dot{I}_{rD1ref}$ and $\dot{I}_{rQ1ref}$ are expected to remain constant and have a very low value. As a result, they might be overlooked. Equation (20) becomes

$$\begin{cases} \dot{s}_d = k_{pd} \times \dot{I}_{rD1} + k_{id\ 0} D_t^{\alpha} \text{sign}\left(e_d\right)^{\gamma} \\ \dot{s}_q = k_{pq} \times \dot{I}_{rQ1} + k_{iq\ 0} D_t^{\alpha} \text{sign}\left(e_q\right)^{\gamma} \end{cases}. \tag{20}$$

Now replacing the value of $\dot{I}_{rD1f}$ from Eq. (2) into Eq. (20) and considering k_{pd} modest and easily overlooked.

$$\begin{cases} \dot{s}_d = F_d\left(.\right) + zm_d + \sigma_d + k_{id\ 0} D_t^{\alpha} \text{sign}\left(e_d\right)^{\gamma} \\ \dot{s}_q = F_q\left(.\right) + zm_q + \sigma_q + k_{iq\ 0} D_t^{\alpha} \text{sign}\left(e_q\right)^{\gamma} \end{cases} \tag{21}$$

The control rule made sure that the reference current tracking signal was on the sliding surface for PWM to create the gate signal employing the FOSMC condition.

$$\begin{cases} m_d = \dfrac{-\left[F_d\left(.\right) + k_d \text{sign}\left(s_d\right) + k_{id\ 0} D_t^{\alpha} \text{sign}\left(e_d\right)^{\gamma}\right]}{z} \\ m_q = \dfrac{-\left[F_q\left(.\right) + k_q \text{sign}\left(s_q\right) + k_{iq\ 0} D_t^{\alpha} \text{sign}\left(e_q\right)^{\gamma}\right]}{z} \end{cases} \tag{22}$$

The terms k_d and k_q denote sliding gains:

$$\begin{aligned} &s_{dq}\left(t\right) = k_{pdq} \times \dot{e}_{dq}\left(t\right) + k_{idq} \times {}_0D_t^{\alpha-1} e_{dq}\left(t\right), \\ &k_{pdq}, k_{idq} > 0 \quad 0 < \alpha < 1. \end{aligned} \tag{23}$$

More importantly, the FSMC approach's stability is then theoretically examined using the Lyapunov theory [12]. The Lyapunov candidate function for FSMC stability in grid-connected means is defined as:

$$V\left(t\right) = \frac{s_d^2 + s_q^2}{2}. \tag{24}$$

Differentiating $V(t)$ with regard to time t in Eq. (12) and replacing Eq. (21) into Eq. (24), Eq. (25) becomes:

$$\begin{aligned} &\dot{V}\left(t\right) = s_d \times \dot{s}_d + s_q \times \dot{s}_q \\ &= s_d\left(k_{pd} \times \dot{I}_{rD1} + k_{id\ 0} D_t^{1-\alpha} \text{sign}\left(e_d\right)^{\gamma}\right) \\ &+ s_q\left(k_{pq} \times \dot{I}_{rQ1} + k_{iq\ 0} D_t^{1-\alpha} \text{sign}\left(e_q\right)^{\gamma}\right) \\ &= s_d\left(-\sigma_d - k_d \text{sign}\left(s_d\right)\right) + s_q\left(-\sigma_q - k_q \text{sign}\left(s_q\right)\right). \end{aligned} \tag{25}$$

Considering $\text{sign}(S_d) = |S_d|/S_d$. Equation (25) becomes

$$\dot{V}\left(t\right) = \left(S_d \times \sigma_d - k_d \times \left|S_d\right|\right) + \left(S_q \times \sigma_q - k_q \times \left|S_q\right|\right). \tag{26}$$

Considering ($k_d = |\sigma_d| + \zeta_d$) and ($k_q = |\sigma_q| + \zeta_q$), where ζ_d and ζ_q are positive parameters.

$$\begin{aligned} &\dot{V}\left(t\right) \le -\zeta_d \left|S_d\right| - \zeta_q \left|S_q\right| \le -\min\left(\zeta_d \times \zeta_q\right)\left(\left|S_d\right| + \left|S_q\right|\right) \\ &= -\min\left(\zeta_d \times \zeta_q\right)\left\|S\right\|_1 \end{aligned} \tag{27}$$

The minimum (ζ_d, ζ_q) represents the ζ_d and ζ_q minimum values. Equation (22) establishes the stability condition and shows the convergence of a sliding surface in finite time.

3.3 Adaptive Hierarchical Fractional Sliding Mode Controller (AHFSMC)

In this study, an adaptive hierarchical sliding mode controller is developed. This method divides an unresponsive system into several subsystems based on its physical structure. Then, as the first layer sliding surface, the sliding surface of one HSMC for the converter side MtVDC system is chosen. It is used to connect the sliding surface of the second layer to the sliding surface of alternative subsystem. This process is repeated until all of the subsystem sliding surfaces have been included. The total control law is given as:

$$u\left(t\right) = u_{sl}\left(t\right) + u_{sw}\left(t\right) + u_{cc}\left(t\right), \tag{28}$$

where the sliding control law is $u_{sl}(t)$ which is obtained from the system's first layer sliding surface, the approach control law is $u_{sw}(t)$ and the corrective control law is $u_{cc}(t)$. The AHFSMC's first layer sliding surfaces are designed for the test system under total control law is defined as:

$$\begin{cases} s_1\left(t\right) = \begin{cases} s_{d1}\left(t\right) = k_{pd1} \times \dot{e}_{d1}\left(t\right) + k_{id1} \times {}_0D_t^{\alpha-1} e_{d1}\left(t\right), \\ k_{pd1}, k_{id1} > 0, \ 0 < \alpha < 1 \\ s_{q1}\left(t\right) = k_{pq1} \times \dot{e}_{q1}\left(t\right) + k_{iq1} \times {}_0D_t^{\alpha-1} e_{q1}\left(t\right), \\ k_{pq1}, k_{iq1} > 0, \ 0 < \alpha < 1 \end{cases} \\ s_2\left(t\right) = \begin{cases} s_{d2}\left(t\right) = k_{pd2} \times \dot{e}_{d2}\left(t\right) + k_{id2} \times {}_0D_t^{\alpha-1} e_{d2}\left(t\right), \\ k_{pd2}, k_{id2} > 0, \ 0 < \alpha < 1 \\ s_{q2}(t) = k_{pq2} \times \dot{e}_{q2}(t) + k_{iq2} \times {}_0D_t^{\alpha-1} e_{q2}(t), \\ k_{pq2}, k_{iq2} > 0, \ 0 < \alpha < 1 \end{cases} \end{cases}. \tag{29}$$

Two derivatives of Eq. (15) have been computed about time using fractional calculus and second-order SMC theory. Equation (30) shows how to obtain $\ddot{s}_1(t)$ and $\ddot{s}_2(t)$:

$$\begin{cases} \ddot{s}_1\left(t\right) = \begin{cases} \ddot{s}_{d1}\left(t\right) = k_{pd1} \times \ddot{e}_{d1}\left(t\right) + k_{id1} \times {}_0D_t^{\alpha-2} e_{d1}\left(t\right), \\ \ddot{s}_{q1}\left(t\right) = k_{pq1} \times \ddot{e}_{q1}\left(t\right) + k_{iq1} \times {}_0D_t^{\alpha-2} e_{q1}\left(t\right), \end{cases} \\ \ddot{s}_2\left(t\right) = \begin{cases} \ddot{s}_{d2}\left(t\right) = k_{pd2} \times \ddot{e}_{d2}\left(t\right) + k_{id2} \times {}_0D_t^{\alpha-2} e_{d2}\left(t\right), \\ \ddot{s}_{q2}\left(t\right) = k_{pq2} \times \ddot{e}_{q2}\left(t\right) + k_{iq2} \times {}_0D_t^{\alpha-2} e_{q2}\left(t\right) \end{cases} \end{cases}. \tag{30}$$

Using the expression $e_d = I_{rD1}$ and $e_q = I_{rQ1}$ (as I_{rD1ref} and I_{rQ1ref} are very small) and then substituting the value of I_{rD1} and I_{rQ1} and $e_d = \text{sign}(e_d)^{\gamma}$ in Eq. (30) with Eq. (21), we get the Eq. (31):

$$\begin{cases} \ddot{s}_1(t) = \begin{cases} \ddot{s}_{d1}(t) = \ddot{F}_{d1}(.) + z_1 m_d + \sigma_d \\ +k_{id1} \times {}_0D_t^{\alpha-2}\left(\text{sign}\left(e_{d1}\right)^{\gamma}\right), \\ \ddot{s}_{q1}(t) = \ddot{F}_{q1}(.) + z_1 m_q + \sigma_q \\ +k_{iq1} \times {}_0D_t^{\alpha-2}\left(\text{sign}\left(e_{q1}\right)^{\gamma}\right), \end{cases} \\ \ddot{s}_2(t) = \begin{cases} \ddot{s}_{d2}(t) = \ddot{F}_{d2}(.) + z_2 m_d + \sigma_d \\ +k_{id2} \times {}_0D_t^{\alpha-2}\left(\text{sign}\left(e_{d2}\right)^{\gamma}\right), \\ \ddot{s}_{q2}(t) = \ddot{F}_{q2}(.) + z_2 m_q + \sigma_q \\ +k_{iq2} \times {}_0D_t^{\alpha-2}\left(\text{sign}\left(e_{q2}\right)^{\gamma}\right) \end{cases} \end{cases}. \tag{31}$$

The SMC is second-order if its first and second derivatives with the sliding surface are zero. As a result, if $\ddot{s}_1(t) = \ddot{s}_2(t) = 0$, then the control laws for two subsystems becomes Eq. (32):

$$\begin{cases} u_{me1}(t) = \begin{cases} m_{d1}(t) = -z_1^{-1}\left[\ddot{F}_{d1}(.) + \sigma_{d1}\right. \\ \left.+k_{id1} \times {}_0D_t^{\alpha-2}\left(\text{sign}\left(e_{d1}\right)^{\gamma}\right)\right], \\ m_{q1}(t) = -z_1^{-1}\left[\ddot{F}_{q1}(.) + \sigma_{q1}\right. \\ \left.+k_{iq1} \times {}_0D_t^{\alpha-2}\left(\text{sign}\left(e_{q1}\right)^{\gamma}\right)\right], \end{cases} \\ u_{me2}(t) = \begin{cases} m_{d2}(t) = -z_2^{-1}\left[\ddot{F}_{d2}(.) + \sigma_{d2}\right. \\ \left.+k_{id2} \times {}_0D_t^{\alpha-2}\left(\text{sign}\left(e_{d2}\right)^{\gamma}\right)\right], \\ m_{q2}(t) = -z_2^{-1}\left[\ddot{F}_{q2}(.) + \sigma_{q2}\right. \\ \left.+k_{iq2} \times {}_0D_t^{\alpha-2}\left(\text{sign}\left(e_{q2}\right)^{\gamma}\right)\right] \end{cases} \end{cases}. \tag{32}$$

Control rules for each subsystem m_{ei} shown in Eq. (32) can only cause the subsystem to get to the sliding surface of the first layer, according to the HFSMC principle. The stable control law $m_{ei\text{-}s}$ is added as a feedback element of the subsystem control law to increase the resilience against unknown disturbance and chattering in the test system at the subsystem level. The subsystem m_{ei}'s control law has been revised in Eq. (33):

$$\begin{cases} u_{me1}(t) = \begin{cases} m_{d1}(t) = -z_1^{-1}\left[\ddot{F}_{d1}(.) + \sigma_{d1}\right. \\ \left.+k_{id1} \times {}_0D_t^{\alpha-2}\left(\text{sign}\left(e_{d1}\right)^{\gamma}\right)\right] + m_{d1-s(t)}, \\ m_{q1}(t) = -z_1^{-1}\left[\ddot{F}_{q1}(.) + \sigma_{q1}\right. \\ \left.+k_{iq1} \times {}_0D_t^{\alpha-2}\left(\text{sign}\left(e_{q1}\right)^{\gamma}\right)\right] + m_{q1-s(t)}, \end{cases} \\ u_{me2}(t) = \begin{cases} m_{d2}(t) = -z_2^{-1}\left[\ddot{F}_{d2}(.) + \sigma_{d2}\right. \\ \left.+k_{id2} \times {}_0D_t^{\alpha-2}\left(\text{sign}\left(e_{d2}\right)^{\gamma}\right)\right] + m_{d2-s(t)}, \\ m_{q2}(t) = -z_2^{-1}\left[\ddot{F}_{q2}(.) + \sigma_{q2}\right. \\ \left.+k_{iq2} \times {}_0D_t^{\alpha-2}\left(\text{sign}\left(e_{q2}\right)^{\gamma}\right)\right] + m_{q2-s(t)} \end{cases} \end{cases}. \tag{33}$$

The following statement for the stable control law has been chosen in the subsystem control law $m_{ei\text{-}s(t)}$.

$$m_{ei-s(t)} = -z_i(t)^{-1}\left(\mu_i \text{sign}\left(\dot{s}_i\right) + \eta_i\left(s_i\right)\right), \tag{34}$$

where μ_i and η_i are stable gain values.

The subsystem control law can be represented as Eq. (33) and Eq. (34). The controller exhibits considerable robustness when the stable gain of the subsystem control law is bigger than the top bound of unknown disturbances. The flaws of the subsystems in the control process will be overlaid and linked with the system's overall control law when confronted with HSMC and is particularly destructive to the MtVDC system. As a consequence, an adaptive estimation of its 1st derivative is presented and given in Eq. (35) based on the stable gain parameters μ_i and η_i of the subsystem stable control law $m_{ei\text{-}s(t)}$:

$$\begin{matrix} \dot{\hat{\mu}} = \rho_i s \times \text{sign}\left(\dot{s}_i\right) \\ \dot{\hat{\lambda}} = \kappa_i s \times s_i \end{matrix}, \tag{35}$$

where $\dot{\hat{\mu}}$ and $\dot{\hat{\lambda}}$ are the stable gain parameters' adaptive constants and both are positive numbers. As a result, the AHFSMC's adaptive subsystem control laws are depicted in Eq. (36):

$$\begin{cases} u_{me1}(t) = \begin{cases} -z_1^{-1}\left[\begin{matrix} \ddot{F}_{d1}(.) + k_{id1}\left({}_0D_t^{\alpha-2}\left(\text{sign}\left(e_{d1}\right)^{\gamma}\right)\right) \\ +\hat{\mu}_{d1}\left(\text{sign}\left(\dot{s}_{d1}\right)\right) + \hat{\eta}_{d1} s_{d1} \end{matrix}\right], \\ -z_1^{-1}\left[\begin{matrix} \ddot{F}_{q1}(.) + k_{iq1}\left({}_0D_t^{\alpha-2}\left(\text{sign}\left(e_{q1}\right)^{\gamma}\right)\right) \\ +\hat{\mu}_{q1}\left(\text{sign}\left(\dot{s}_{q1}\right)\right) + \hat{\eta}_{q1} s_{q1} \end{matrix}\right], \end{cases} \\ u_{me2}(t) = \begin{cases} -z_2^{-1}\left[\begin{matrix} \ddot{F}_{d2}(.) + k_{id2}\left({}_0D_t^{\alpha-2}\left(\text{sign}\left(e_{d2}\right)^{\gamma}\right)\right) \\ +\hat{\mu}_{d2}\left(\text{sign}\left(\dot{s}_{d2}\right)\right) + \hat{\eta}_{d2} s_{d2} \end{matrix}\right], \\ -z_2^{-1}\left[\begin{matrix} \ddot{F}_{q2}(.) + k_{iq2}\left({}_0D_t^{\alpha-2}\left(\text{sign}\left(e_{q2}\right)^{\gamma}\right)\right) \\ +\hat{\mu}_{q2}\left(\text{sign}\left(\dot{s}_{q2}\right)\right) + \hat{\eta}_{q2} s_{q2} \end{matrix}\right] \end{cases} \end{cases}. \tag{36}$$

The $s(t)$ is the second layer sliding surface:

$$s(t) = c_1 \dot{s}_1(t) + c_2 \dot{s}_2(t), \tag{37}$$

where $c_1 > 0$ and $c_2 > 0$. Using the adaptive subsystem control principles, $\dot{s}(t)$ can be computed as:

$$\begin{cases} \dot{s}_d(t) = \ddot{s}_{d1}(t) + c_2 \ddot{s}_{d2}(t) \\ \dot{s}_q(t) = \ddot{s}_{q1}(t) + c_2 \ddot{s}_{q2}(t) \end{cases}. \tag{38}$$

To design the AHFSMC (Fig. 3), the exponential approach law has been used, as shown in Eq. (36), to make the second sliding variable $s(t)$ rapidly converge to 0:

$$\dot{s}(t) = -\varepsilon_1 s + \varepsilon_2 \text{sign}(s), \tag{39}$$

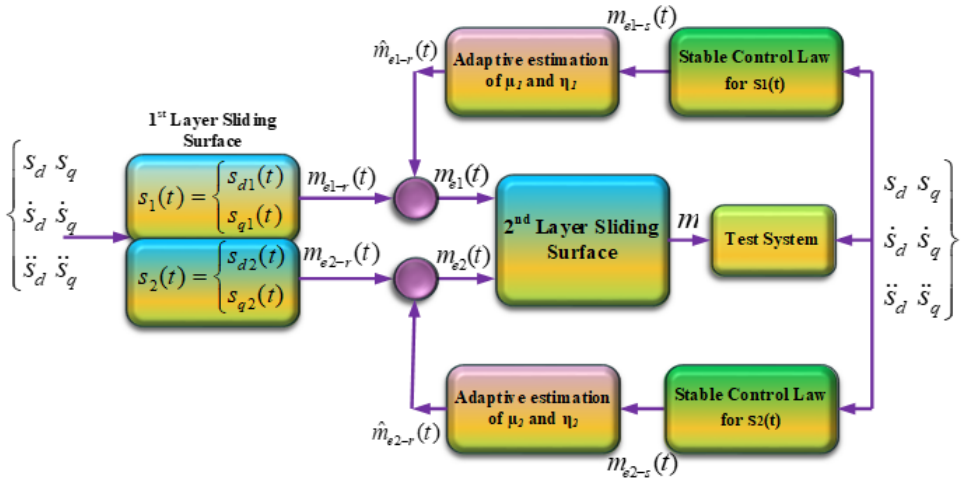

Fig. 3 The structure of the AHFSMC

where ε_1, ε_2 are greater-than-zero constants. The approach control law $u_{sw}(t)$ can be calculated using Eq. (38) and Eq. (39). The following theorems from the AHFSMC can be derived:

$$u_{sw}(t)=\frac{c_2z_2m_{x2}}{c_1z_1+c_2z_2}-\frac{c_1z_1m_{x1}}{c_1z_1+c_2z_2}+\frac{\varepsilon_1 s+\varepsilon_2\operatorname{sign}(s)}{c_1z_1+c_2z_2}\Bigg|_{x=d,q} \quad (40)$$

By bringing Eq. (40) into Eq. (22), the control law of AHFSMC can be derived as:

$$\begin{cases} u(t)=u_{me1}(t)+u_{me2}(t)+u_{sw}(t) \\ =\dfrac{c_1z_1m_{x1}}{c_1z_1+c_2z_2}+\dfrac{c_2z_2m_{x2}}{c_1z_1+c_2z_2}+\dfrac{\varepsilon_1 s+\varepsilon_2\operatorname{sign}(s)}{c_1z_1+c_2z_2}\Bigg|_{x=d,q} \end{cases}. \quad (41)$$

Theorem 1: Assume that the desired control action of the test system is a continuous and bounded function. If Eq. (36) is taken as the control law of the subsystems and Eq. (41) is taken as the control law of the total system, then *lim D* = 0 can be realized for the test system with the dynamic model shown in Eq. (22).

Lemma 1: Consider the following Lyapunov candidate function

$$V=\frac{s^2}{2}+\sum_{i=1}^{2}\left(\frac{\hat{\eta}_i^2}{2\kappa_i}+\frac{c_iz_i\hat{\mu}_i^2}{2\rho_i}\right)\Bigg|_{d,q}. \quad (42)$$

The time derivative of the Lyapunov candidate function becomes

$$\begin{aligned} \dot{V}&=s\times\dot{s}+\frac{1}{\kappa_1}\hat{\eta}_1\dot{\hat{\eta}}_1+\frac{1}{\kappa_2}\eta_2\dot{\hat{\eta}}_2 \\ &+\frac{2c_1z_1}{\rho_1}\mu_1\dot{\mu}_1+\frac{2c_2z_2}{\rho_2}\mu_2\dot{\mu}_2 \\ &=\begin{bmatrix} s\times\dot{s}+\eta_1 s\times\dot{s}_1+\eta_2 s\times\dot{s}_2+2c_1z_1\mu_1 s\times\operatorname{sign}(\dot{s}_1) \\ +2c_2z_2\mu_2 s\times\operatorname{sign}(\dot{s}_2) \end{bmatrix}\Bigg|_{d,q}, \end{aligned} \quad (43)$$

where $\dot{V}$ is a positive definite derivative function with a negative semi-definite derivative. By bringing Eq. (41) into Eq. (42) results

$$\begin{aligned} \dot{V}&=s\begin{bmatrix} \varepsilon_1 s-\varepsilon_2\operatorname{sign}(s)-\eta_1\hat{s}_1 \\ +\eta_2\hat{s}_2-c_1z_1\mu_1\operatorname{sign}(\dot{s}_1) \\ -c_2z_2\mu_2\operatorname{sign}(\dot{s}_2) \end{bmatrix}\Bigg|_{d,q} \\ &+\begin{bmatrix} \eta_1 s\times s_1+\eta_2 s\times s_2+c_1z_1\mu_1 s\times\operatorname{sign}(\dot{s}_1) \\ +c_2z_2\mu_2 s\times\operatorname{sign}(\dot{s}_2) \end{bmatrix}\Bigg|_{d,q}. \end{aligned} \quad (44)$$

Lemma 2: Consider the following Lyapunov candidate function

$$V=\frac{s_i^2}{2}+\frac{\dot{s}_i^2}{2}. \quad (45)$$

In the first section, we will show that s_1, $s_2 \in L_2$, i.e.

$$\int_0^\infty s_1^2(t)\,dt<\infty,\ \int_0^\infty s_2^2(t)\,dt<\infty \quad (46)$$

Integrating both sides of Eq. (45) yields,

$$\int_0^t\dot{V}(\tau)\,d\tau=V(t)-V(0)=-\int_0^t ks^2(\tau)\,d\tau-\int_0^t\mu|s|(\tau)\,d\tau \quad (47)$$

$$\begin{aligned} V(t)&=\frac{s^2}{2}=V(0)-\int_0^t ks^2(\tau)\,d\tau-\int_0^t\mu|s|(\tau)\,d\tau \\ &\le V(0)<\infty. \end{aligned} \quad (48)$$

According to Eq. (20) and Eq. (47), we have

$$\alpha^2\int_0^\infty s_1^2(t)\,dt+\int_0^\infty 2\alpha\beta s_1(t)s_2(t)\,dt+\beta^2\int_0^\infty s_2^2(t)\,dt<\infty \quad (49)$$

$$\int_0^\infty s^2(t)\,dt=\int_0^\infty\left(\alpha^2s_1^2(t)+2\alpha\beta s_1(t)s_2(t)+\beta^2s_2^2(t)\right)dt<\infty. \quad (50)$$

Equation (45) states that $\alpha\beta s_1(t)s_2(t)>0$. This means that the inequality Eq. (49) has three positive terms on the left side. As a result, all of these terms should be constrained. As a result, condition Eq. (46) should be met. In the second part of the proof, we will demonstrate that s_1, $s_2 \in L_\infty$, s_1, $s_2 \in L_\infty$. According to Eq. (46), $s \in L_\infty$. Moreover, based on Eq. (44), $s \in L_\infty$. On the other hand, taking into account , since $s \in L_\infty$ s_1, $s_2 \in L_\infty$. Since the terms in s_1 and s_2's right-hand parts are finite, so,

$$Sup|\dot{s}_1| = \|\dot{s}_1\|_\infty < \infty, \quad Sup|\dot{s}_2| = \|\dot{s}_2\|_\infty < \infty. \tag{51}$$

Finally, the asymptotic stability of the system Eq. (51) is guaranteed by Lemma 2.

4 Result analysis

In the proposed approach instead of the WF, the constant voltage source is studied. The performance of the proposed approach AHFSMC is justified under various conditions and the performance is justified with the comparative simulative result with analyzing the performance based on time-domain analysis and percentage of improvement.

4.1 Load step change at VSC-1 (Case 1)

To see how well AHFSMC performs in the face of system uncertainty, VSC-1 is subjected to a 10% load increase in a short period (0.75 sec). The impact of this fluctuation on system performance is depicted in Fig. 4. The control of AHFSMC results in a satisfactory dynamic response.

4.2 Active and reactive power variation (Case 1)

Under the same operating conditions as discussed above, a step-change in the active power reference is presented. The proposed controller restores the system to its original state faster than the other controllers which is visible in Fig. 5.

To present a quantified value, Table 1 summarises the efficiency of the suggested controller in comparison to the other controllers.

4.3 Voltage ride through ability (Case 2)

As shown in Fig. 6, VSC-1 short-circuit faults cause a large voltage deviation on the dc side.

4.4 Active and reactive power variation (Case 2)

Under the same operating conditions as discussed above, a step-change in the active power reference is presented, and the response is measured. The proposed controller restores the system to its original state faster than the other controllers which has been clearly demonstrated in Fig. 7.

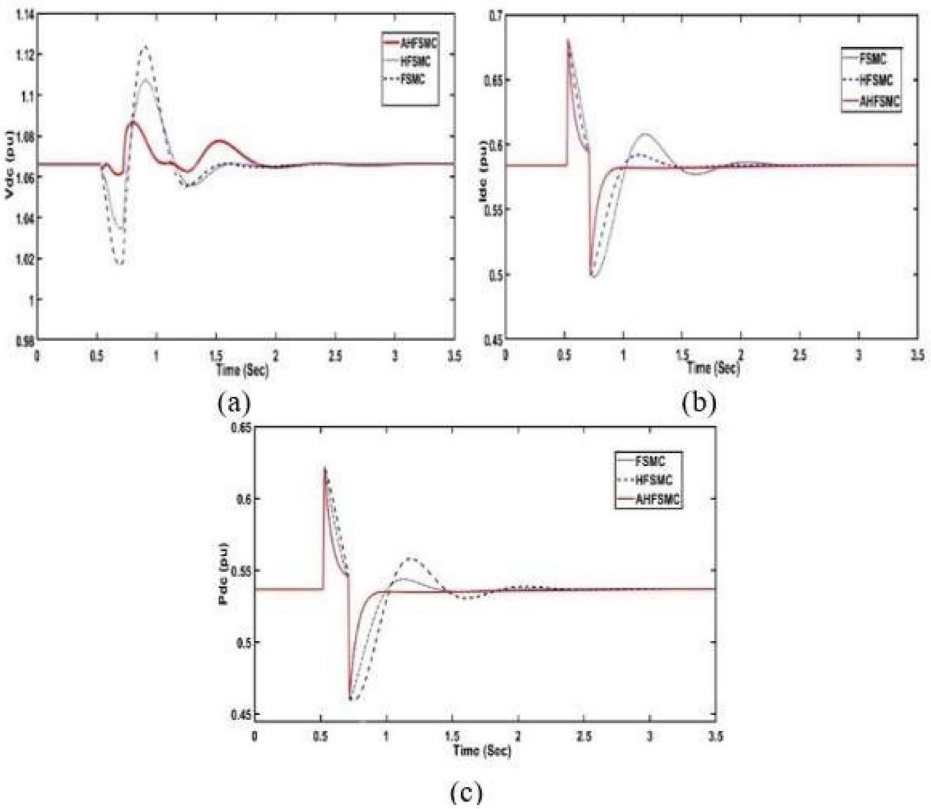

Fig. 4 Controller's performance of the MtVDC systems

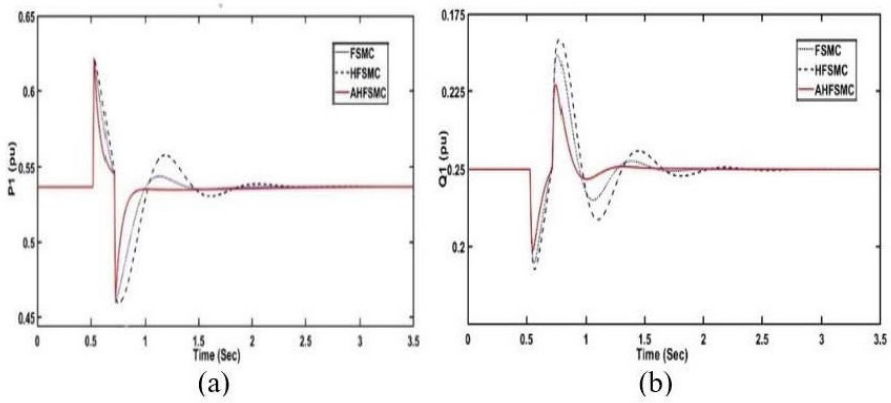

Fig. 5 The active and reactive power outputs of VSC-1

Table 1 The test system's time domain analysis for Case 1

Performance	Characteristics	FSMC	HFSMC	AHFSMC
Peak value (pu)	V_{dc}	1.12	1.107	1.09
	I_{dc}	0.687	0.685	0.68
	P_{dc}	0.6816	0.6814	0.6811
	P_1	0.638	0.636	0.625
	Q_1	0.265	0.255	0.225
Settling time (sec)	V_{dc}	2.9	2.78	2.62
	I_{dc}	2.32	1.5	0.82
	P_{dc}	2.79	2.43	1.16
	P_1	2.72	1.48	0.76
	Q_1	2.57	1.82	1.57

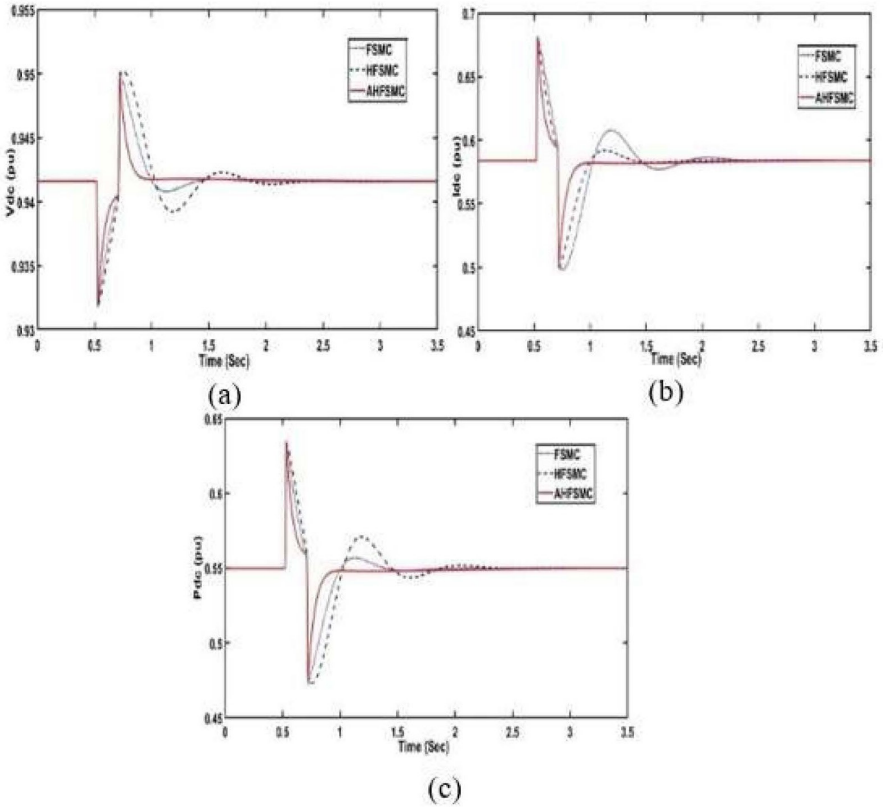

Fig. 6 Controller's performance of MtVDC systems during voltage ride through

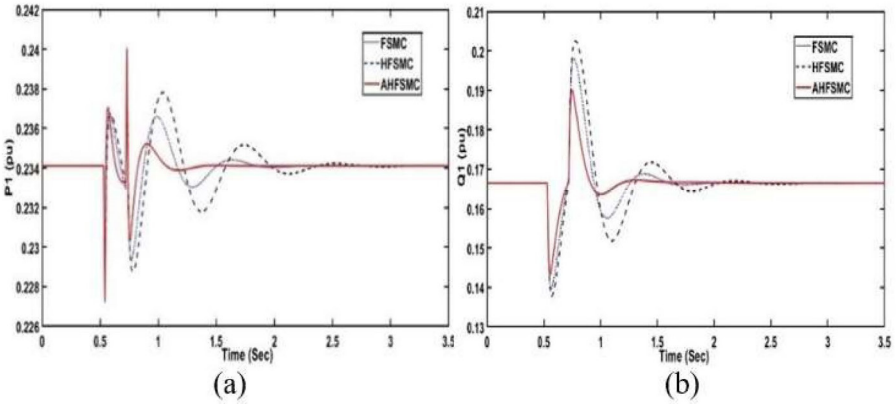

Fig. 7 The active and reactive power outputs of VSC-1

Table 2 The test system's time domain analysis for Case 2

Performance	Characteristics	FSMC	HFSMC	AHFSMC
Peak value (pu)	V_{dc}	0.933	0.932	0.93
	I_{dc}	0.685	0.684	0.682
	P_{dc}	0.634	0.633	0.632
	P_1	0.235	0.235	0.236
	Q_1	0.12	0.14	0.147
Settling time (sec)	V_{dc}	2.43	1.61	1.35
	I_{dc}	2.31	1.47	0.81
	P_{dc}	2.47	1.24	1.18
	P_1	3.21	1.54	0.51
	Q_1	2.72	1.57	1.53

Table 2 shows that the transient stability conditions for peak and settling time are relatively low in the proposed AHFSMC than the other controllers, implying that the transient period is shorter and the oscillations decay faster.

5 Conclusion

In this paper, the proposed Lyapunov-based control strategy solves the problem of enormous voltage angle and equency deviation, ensuring the system's stability and working performance. In particular, the proposed approach with great precision and prompt reaction consider and estimates uncertainties such as external disturbances, measurable errors, and modeling errors, which aids in minimizing the effect of complexities in the controller design stage.

References

[1] International Energy Agency "India Energy Outlook 2021" OECD Publishing, Paris, France, 2021. https://doi.org/10.1787/ec2fd78d-en2021

[2] IWTMA "Wind Power Profile of Madhya Pradesh" [pdf] Indian Wind Turbine Manufacturers Association. Available at: https://www.indianwindpower.com/pdf/Madhya-Pradesh-State-Wind-Power-Profile.pdf [Accessed: 04 February 2023]

[3] Climate Wise "100.5 MW Wind Power Project in Madhya Pradesh, India", [online] Available at: https://climate-wise.com/Projects/100-5-mw-wind-power-project-in-madhya-pradesh-india/ [Accessed: 04 February 2023]

[4] The Wind Power "Mamatkheda (India) - Wind", [online] Available at: https://www.thewindpower.net [Accessed: 04 February 2023]

[5] He, J., Li, B., Li, Y., Wang, W., Lyu, H., Li, B. "Simplified calculation method of threshold value for the non-unit transient-voltage based protection in multi-terminal VSC-HVDC grid", International Journal of Electrical Power & Energy Systems, 134, 107435, 2022. https://doi.org/10.1016/j.ijepes.2021.107435

[6] Chen, Y., Wang, H., Zhu, M., Liu, M., Ma, J.,Cai, X. "Passive Sliding Mode Controlled UPFC and its Treatment Strategy of Unbalanced Grid Conditions", Frontiers in Energy Research, 9, 712397, 2021. https://doi.org/10.3389/fenrg.2021.712397

[7] Biswal, S. S., Swain, D. R., Rout, P. K. "Inter-area and intra-area oscillation damping for UPFC in a multi-machine power system based on tuned fractional PI controllers", International Journal of Dynamics and Control, 10(4), pp 1594–1612, 2022.
https://doi.org/10.1007/s40435-021-00891-4

[8] Fesharaki, J. A., Tabatabaei, M. "Adaptive Hierarchical Fractional-Order Sliding Mode Control of an Inverted Pendulum–Cart System", Arabian Journal for Science and Engineering, 47(11), pp. 13927–13942, 2022.
https://doi.org/10.1007/s13369-022-06613-y

[9] Biswal, S. S., Swain, D. R., Rout, P. K.. "Control of Parallel AC Voltage Source Converter High-Voltage DC System Using an Adaptive PI Evolutionary-Based Controller", Arabian Journal for Science and Engineering, 46(3), pp. 931–945, 2020.
https://doi.org/10.1007/s13369-020-04764-4

[10] Gorenflo, R., Kilbas, A. A., Mainardi, F., Rogosin, S. V. "Mittag-Leffler Functions, Related Topics and Applications", Springer, 2020. ISBN 978-3-662-61549-2
https://doi.org/10.1007/978-3-662-61550-8

[11] Garra, R., Garrappa, R. "The Prabhakar or three parameter Mittag–Leffler function: Theory and application", Communications in Nonlinear Science and Numerical Simulation, 56, pp. 314–329, 2017.
https://doi.org/10.1016/j.cnsns.2017.08.018

[12] Ghandhari, M., Andersson, G., Hiskens, I. A. "Control Lyapunov functions for controllable series devices", IEEE Transactions on Power Systems, 16(4), pp. 689–694, 2001.
https://doi.org/10.1109/59.962414

Appendix

Vbase: 132 kV(ac), 150 kV(dc), Pbase: 100 MVA, Steady-state system parameter values: 16 MW and 10 MVAR, parameters for transmission-line: 0.05 Ω/km, line resistance of the transmission link: R_{dc} = 0.01 Ω/km (50 km Capacitance of DC-Link capacitor: C_{dc} =5000 μF, AC-filters: C_{ac} = 10 μF.